

Initiation mechanism on transverse microstructure and properties inhomogeneity of hot-rolled low-carbon steel plate

Qingsong He¹, Xufeng Zhang¹, Shuang Su², Qinghua Chen¹, Jian Su¹, Ruinan Chen¹,
Bin Tan¹, Chao Xu¹, Xu Huang¹, Qingwei Dai^{1*}

¹*School of Metallurgy and Materials Engineering, Chongqing University of Science and Technology, Chongqing 401331, P. R. China*

²*Basic Courses Department, ALA, Chongqing 401331, P. R. China*

Received 06 July 2021, received in revised form 23 May 2022, accepted 31 May 2022

Abstract

The center and edge of the hot-rolled low-carbon steel plate reflect the inhomogeneity. Five positions along the transverse direction of the steel plate are taken as the research object. This study reveals the root cause of the inhomogeneity of transverse microstructure and properties of hot-rolled low-carbon steel plates. The grain size in the center of the hot-rolled low-carbon steel plate is relatively large, and the grain size at the edge is relatively small. The mechanical properties test shows that the closer the edge, the higher the hardness. The strength along the transverse direction is similar to the shape of W. The finite element simulation results show that the central cooling is slow, and the deformation degree is different in different transverse positions. In conclusion, the main reason for the inhomogeneous microstructure are the various cooling rates of different parts in the transverse direction. The synergistic effect of grain size and alloying elements is the main reason that causes the transverse strength distribution to show a "W" shape.

Key words: low-carbon steel, transverse structure and properties, cooling rate, finite element simulation

1. Introduction

In recent years, with the rapid development of the world economy, a large number of steel plates have been produced and supplied to all walks of life [1, 2]. Hot-rolled low-carbon steel plate is one of the most widely used steel plates because of its simple manufacturing process, low cost, and excellent performance [3]. The performance of hot-rolled low-carbon steel plates is affected by many factors, such as rolling temperature, rolling passes, roll speed, reduction, and cooling rate [4, 5]. These steps are mainly to control the accumulation of dislocations through temperature, deformation, phase transformation, and strain rate, to control the properties of materials [6]. In the annealing process of hot-rolled low-carbon steel plate, a large amount of energy is stored in the rolling process and released through recovery, recrystallization, and grain growth. The grain size, grain distribution, grain ori-

entation, and dislocation structure of steel plates are changed. The evolution of microstructure is closely related to the final mechanical properties of products. Therefore, in the material innovation stage, it is necessary to understand the relationship between the hot working process, microstructure, and material properties, which helps to adjust and control the initial properties of materials [1, 5, 6].

Over the past few years, the research on hot-rolled low-carbon steel mainly focused on controlling the formation of intergranular ferrite to obtain a fine-grained microstructure low-carbon steel plate [7]; the inhomogeneity of increasing distance of fiber texture in the rolling direction and normal direction of rolling surface [8]; the correlation between mechanical properties and retained austenite [9]; and local distribution of orientation relationship and microstructure evolution of lath martensite [10]. At the same time, many researchers predict the stress-strain distribution, tem-

*Corresponding author: tel.: +86-2365023701; e-mail address: daqingwei@cqust.edu.cn

Table 1. The chemical composition of the hot-rolled low-carbon steel plate (wt.%)

	C	Si	Cu	Al	P	S	Cr	B	Fe
Position 1	< 1.5	1.340	0.042	1.020	0.098	0.126	0.079	0.0108	Bal.
Position 2	< 1.5	0.827	0.029	1.440	0.037	0.047	0.050	0.0053	Bal.
Position 3	< 1.5	0.218	0.038	0.405	0.020	0.006	0.013	< 0.001	Bal.
Position 4	< 1.5	0.287	0.039	0.443	0.021	0.008	0.014	< 0.001	Bal.
Position 5	< 1.5	1.080	0.031	> 1.500	0.098	0.126	0.110	0.0203	Bal.

Table 2. The physical properties of Q235 at different temperatures

Temperature (°C)	Thermal conductivity (W m ⁻¹ K ⁻¹)	Density (g cm ⁻³)	Specific heat capacity (J kg ⁻¹ °C ⁻¹)	Poisson's ratio	Coefficient of linear expansion (× 10 ⁻⁵ °C ⁻¹)	Elastic modulus (GPa)
20	50	7.80	460	0.28	1.10	205
250	47	7.70	480	0.29	1.22	187
500	40	7.61	530	0.31	1.39	150
750	27	7.55	675	0.35	1.48	70
1000	30	7.49	670	0.40	1.34	20

perature, and microstructure of hot-rolled steel plates through numerical simulation. For example, the microstructure change of hot-rolled carbon steel can be predicted by the finite element method [11]. A neural network model is established to predict the mechanical properties of steel plate [12]. A two-dimensional finite element model studies the temperature distribution of steel plates [13]. Based on the above simulation basis, we have accumulated experience for future research.

However, with the increasing demand for the precision of steel products, people have great demand for the overall uniformity of steel plates. For example, in the stamping process of automobile shell parts, if the performance of the edges and the core is inconsistent, it will cause the edges of the shell to crack, the deformation of the center will not achieve the expected effect, and finally, the safety of the automobile will be reduced. When a steel plate is used as a load-bearing structural material, if the performance difference at different positions is too significant, it will cause local cracking first, which will affect the overall load-bearing performance. Generally speaking, the stress and strain in the normal direction are not uniform in plastic processing, and the surface and the center of the steel plate are usually in various stress and strain states [14, 15]. In the process of steel plate rolling, the friction between the roll and the surface of the steel plate will produce more significant shear stress. The shear stress decreases gradually from the outside to the inside along the normal direction of the steel plate. The more significant shear stress on the surface of the steel plate can indirectly promote the increase in nucleation rate and decrease in grain size [16]. The difference in carbon content between the surface and the core of the steel plate or the precipitation of carbon will cause the inhomogeneity of

the structure in the region and then affect the mechanical properties of the steel plate [5, 17]. Thus, the carbon content was needed to control to ensure that the rolled metal has excellent mechanical properties, that is, uniform and fine equiaxed grain. In addition, in the heat treatment process of hot-rolled steel plate, the surface of hot-rolled steel plate has a larger contact area with air, the cooling speed is faster, and the heat of the structure in the center is not easy to lose, so the cooling rate is slower [18, 19]. In addition to the above-mentioned inhomogeneity of normal direction microstructure, we found that in the same hot-rolled low-carbon steel plate, the microstructure and mechanical properties of the same thickness in the edge and center are also inhomogeneous. The transverse inhomogeneity of low-carbon steel plate dramatically affects the overall performance and limits its application in many fields. Therefore, it is of great significance to understand the reasons for the transverse inhomogeneous performance of the steel plate to optimize the production process and produce high-quality hot-rolled steel plates.

This study revealed the change in transverse microstructure by observing the microstructure of five typical positions along the transverse direction of a hot-rolled low-carbon steel plate. The fracture morphology was observed to study the difference of cracks at different positions. The strength and hardness are also studied, which shows the inhomogeneity of transverse mechanical properties. The temperature field, stress, and strain of the rolling process were studied by the finite element simulation method. The microstructure, mechanical properties, and cooling rate of low-carbon steel plate are discussed to evaluate the causes of inhomogeneous transverse microstructure and properties.

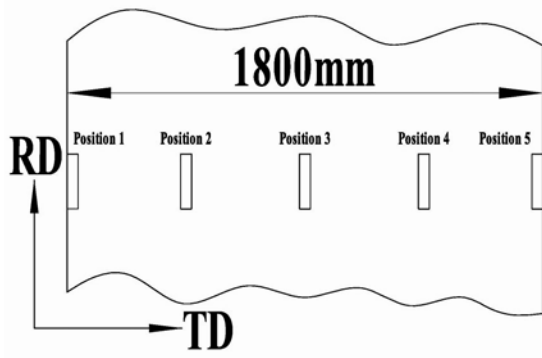


Fig. 1. Location distribution of samples.

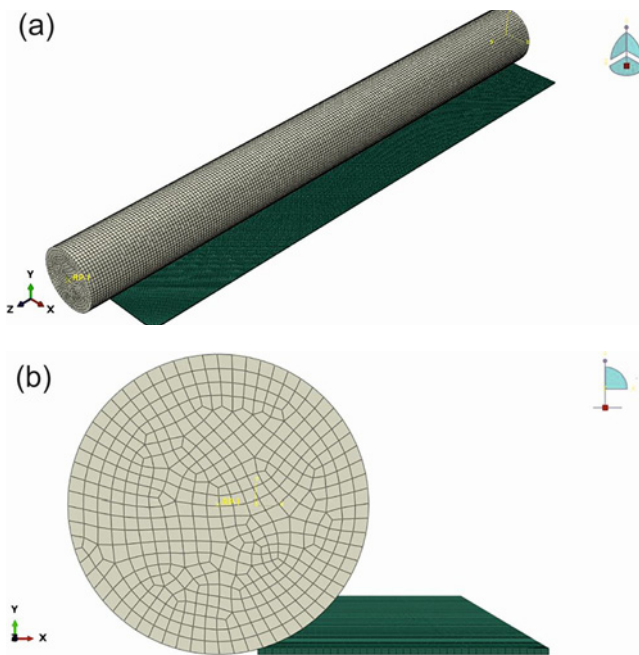


Fig. 2. The finite element rolling model: (a) front view and (b) oblique view.

2. Experimental procedures

The materials used in this study are hot-rolled low-carbon steel plates with a width of 1800 mm and thickness of 4.5 mm in the same production batch. In the transverse direction, five samples from left to right are obtained by wire-electrode cutting, named Position 1, Position 2, Position 3, Position 4, and Position 5, respectively. As shown in Fig. 1, Position 3 is in the center, Position 1 and Position 5 are in the edge, Position 2 and Position 4 are between the edge and the center.

For chemical composition tests, five different positions of the sample were marked, and the average value of chemical composition was obtained by the

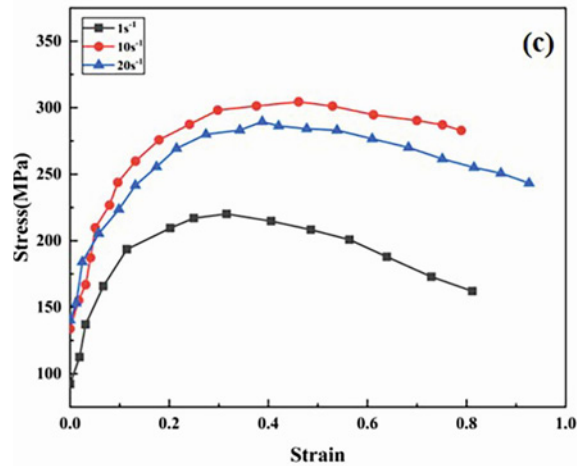
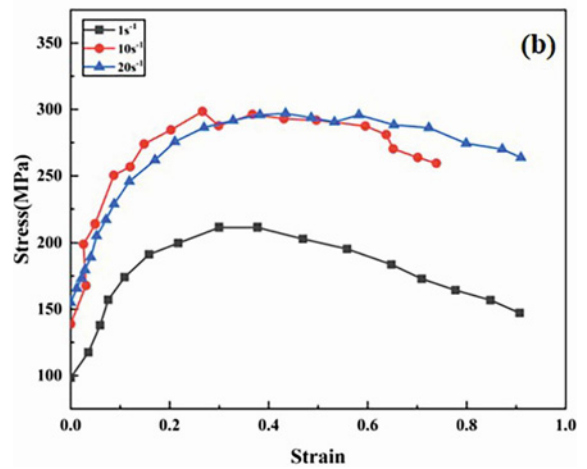
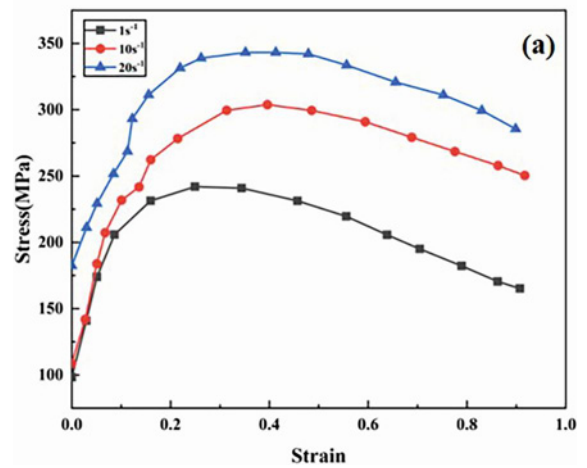


Fig. 3. The stress-strain parameters of Q235 steel at different temperatures: (a) 750 °C, (b) 800 °C, and (c) 850 °C; [20].

FOUNDRY-MASTER PRO spectrometer. The chemical composition is given in Table 1. The microstructure was observed by optical microscope and scanning electron microscope, namely the HITACHI S-3700N emission scanning electron microscope and LEICA

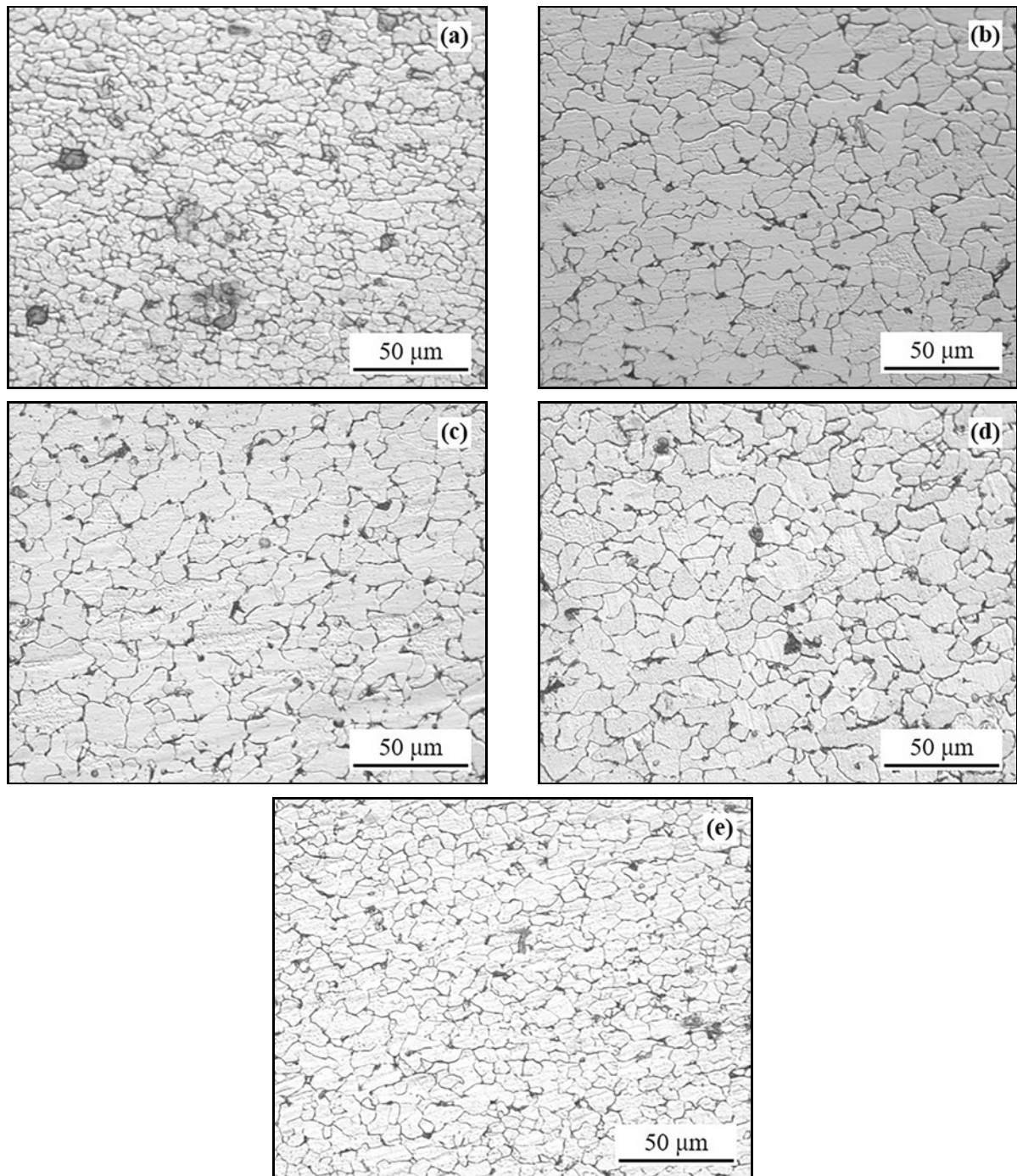


Fig. 4. Optical microstructure of hot-rolled low-carbon steel plate: (a) Position 1, (b) Position 2, (c) Position 3, (d) Position 4, and (e) Position 5.

DM2500M optical microscope. The hardness of the sample was measured by HRS-150 Digital Rockwell Hardness Tester. The yield strength, tensile strength, and elongation were measured by high-temperature tensile testing machines.

The finite element analysis was carried out by the simulation software ABAQUS. The simulation process includes modeling, material properties, assembly, analysis steps, interaction, load, mesh, job, and result

analysis. On the premise of not affecting the simulation results, to save the calculation time, the symmetry plane is established in the RD-TD plane of the plate. The friction coefficient of the material is 0.2, the heat transfer coefficient is 0.17, the ambient temperature is 20 °C, the initial roller temperature is 200 °C, and the initial plate temperature is 820 °C. Table 2 [20] shows the physical properties at different temperatures. Figure 2 shows the rolling model of finite ele-

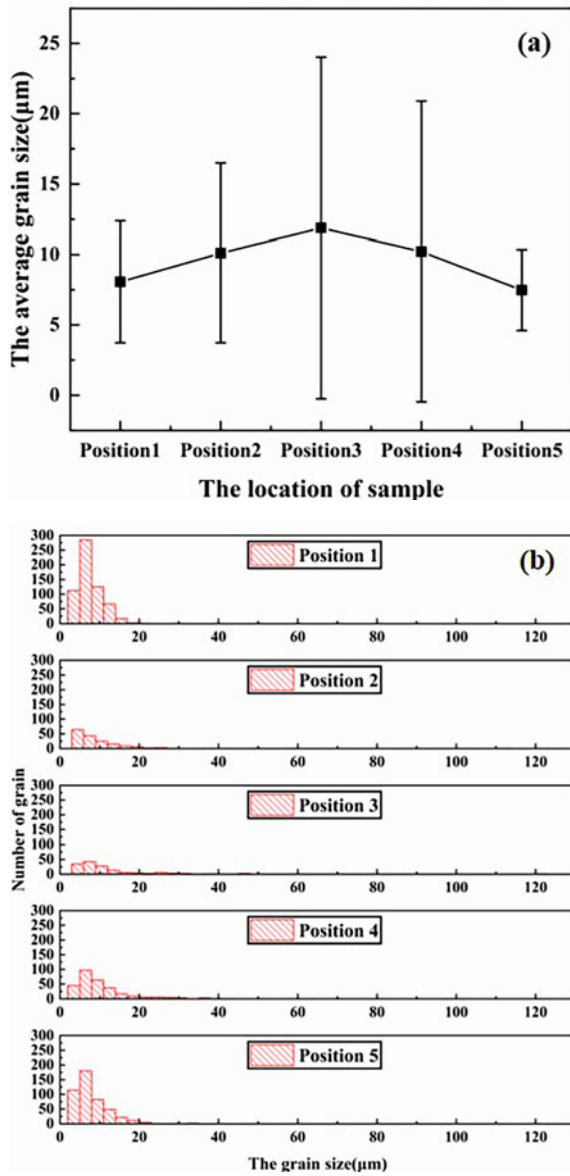


Fig. 5. The grain size of hot-rolled low-carbon steel plate: (a) average grain size at different positions and (b) statistical histogram of grain size at different positions.

ment simulation. Figure 3 [20] shows the stress-strain curves of the material at different temperatures.

3. Results

3.1. Transverse microstructure of hot-rolled low-carbon steel sheet

Figure 4 shows the optical microscope (OM) microstructure of hot-rolled low-carbon steel plate specimens in Position 1, Position 2, Position 3, Position 4, and Position 5, respectively. The microstructure distribution is white equiaxed ferrite and black pearlite,

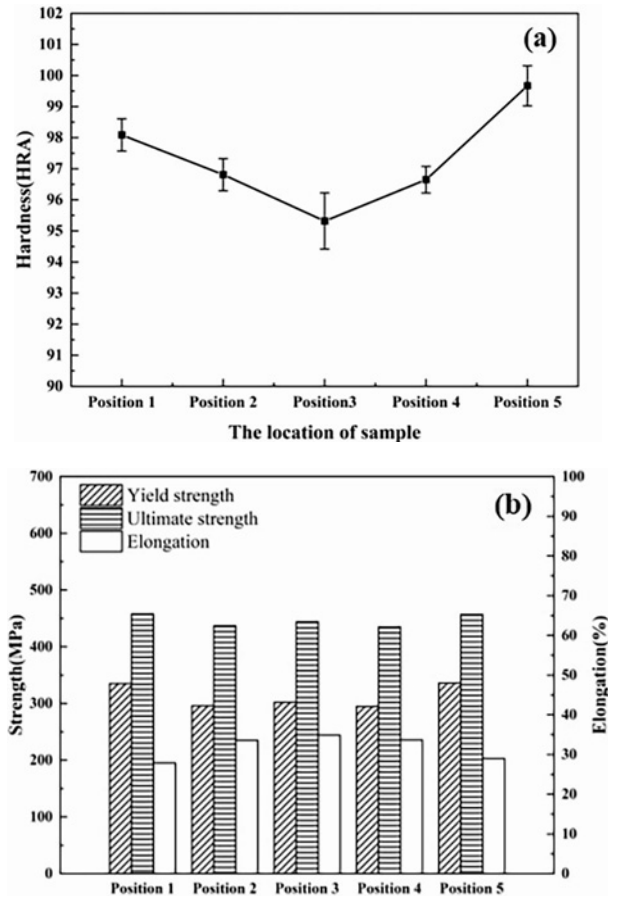


Fig. 6. Mechanical properties of hot-rolled low-carbon steel at different Positions: (a) hardness, (b) yield strength, ultimate strength, elongation.

and the inhomogeneity is mainly reflected in the grain size. The grain size of Position 1 and Position 5 samples is smaller, while the grain size of Position 3 in the middle center is relatively larger. The grain size of Position 2 and Position 4 is between the center and the edge.

To further describe the inhomogeneity of transverse grain size, simultaneously to study the grain size at different positions more intuitively, the microstructure of each sample was selected, and the grain size was quantitatively obtained. The average grain size of Position 1, Position 2, Position 3, Position 4, and Position 5 is $8.0630 \pm 4.330 \mu\text{m}$, $10.1155 \pm 6.381 \mu\text{m}$, $11.8792 \pm 6.381 \mu\text{m}$, $10.2175 \pm 10.691 \mu\text{m}$, $7.4776 \pm 2.882 \mu\text{m}$. Figure 5a shows the average grain size comparison. The broken line trend shows that the average grain size is larger in the middle, and the closer to the edge, the smaller the grain size. The study also found a large gap in the uniformity of grain size at different positions. The particle size span of the central part is large, which indicates that the structure of the central part of the after-rolling plate is slow to dissipate

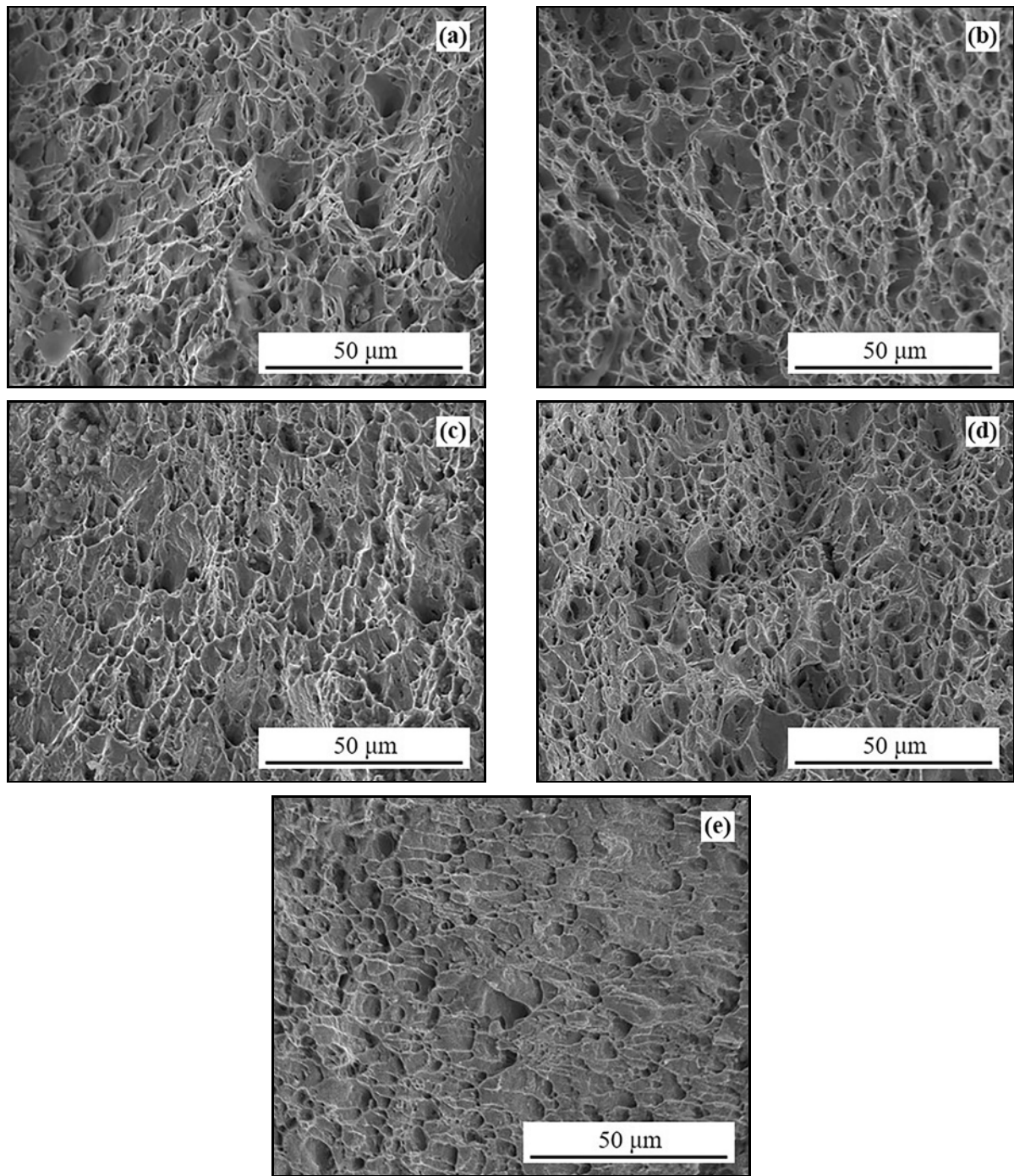


Fig. 7. SEM microstructure of hot-rolled low-carbon steel plate: (a) Position 1, (b) Position 2, (c) Position 3, (d) Position 4, and (e) Position 5.

heat. The heat accumulates in the center to maintain a high-temperature state, which is equivalent to keeping the center in a heat-preservation state for a short time. The growth time of the grain increases and the grain size becomes coarser. As shown in Fig. 5b, the grain size of Position 1 and Position 5 is mainly in size range of 0–20 μm , which indicates that the grain size is homogeneous. However, the grain size of Position 3 is mainly concentrated in the range of 0–20 μm , and

a small amount is concentrated in the range of 20–50 μm , the distribution range is the widest, the number of grains is the lowest, and the uniformity is the lowest. The grain size and homogeneity of Position 2 and Position 4 are between the edge and the center. This is consistent with the previous conclusion: the closer the center, the larger the grain diameter; the less the number of grains, the lower grain distribution uniformity.

3.2. Transverse mechanical properties of hot-rolled low-carbon steel sheet

In this experiment, the sample is a hot-rolled low-carbon steel plate, and the scale is HRA. According to the experimental results, the average hardness values of Position 1, Position 2, Position 3, Position 4, and Position 5 are 98.09 ± 0.52 HRA, 96.81 ± 0.52 HRA, 95.32 ± 0.93 HRA, 96.65 ± 0.43 HRA, and 99.67 ± 0.64 HRA, respectively. The mechanical properties of materials are closely related to the microstructure. Under a specific volume, when the deformation is the same, the smaller the grain size, the greater the grain number. In this case, the deformation will be carried out in finer grain so that the smaller the deformation of each grain, the more uniform it is. As shown in Fig. 6a, it is evident that the hardness in the center is the smallest, and the closer to the edge, the higher the hardness. At the same time, the fluctuation range of the center hardness is the widest, indicating that the hardness in the center is in an unstable state and the uniformity is low. This result is consistent with the uniformity of grain distribution as mentioned above. Moreover, in the transverse direction of the low-carbon steel plate, the grain is not uniform, and the hardness of the center part is different from that of the edge.

Figure 6b shows the elongation, tensile strength, and yield strength of the sample at different locations. As shown in the figure, the closer the center, the better the ductility. The yield strength (σ_s) and tensile strength (σ_b) present a trend similar to the W shape. The strength of Positions 1 and 5 at the edge is the highest, followed by Position 3 at the center. Positions 2 and 4 are the lowest.

3.3. Transverse fracture morphology of hot-rolled low-carbon steel sheet

Figure 7 shows the tensile fracture morphology at different positions. The results show that the fracture morphology of the center and the edges is different. In Fig. 7a, a large dimple is surrounded by a large number of small dimples. The size difference between adjacent dimples is too significant, and the homogeneity is poor. In particular, a giant dimple appears on the right side of Fig. 7a. This indicates that Position 1 is easy to fracture and has poor elongation. In Fig. 7e, the dimples on the right fracture surface are shear and oval. On the left is the common equiaxed dimple. The distribution of dimples on the left and right sides is different, similar to the transition from brittle fracture to ductile fracture. This indicates that the organization of the material at the edge is inhomogeneous, leading to the first partial cracking on the right side of Position 5, and then the entire material is fractured. Therefore, the fracture toughness of Posi-

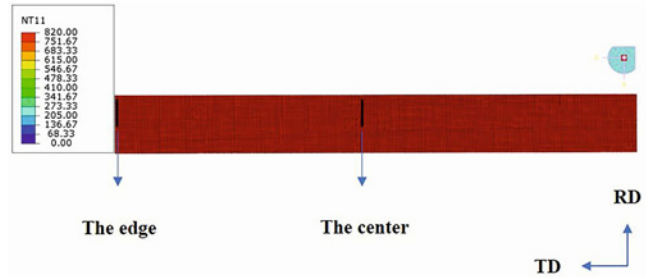


Fig. 8. Areas for observing temperature changes.

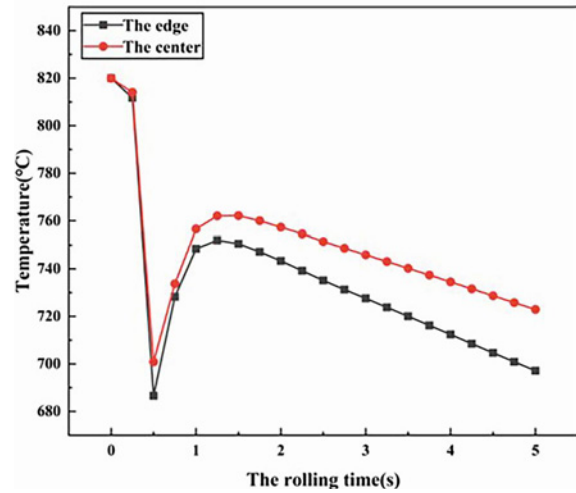


Fig. 9. The curve of temperature changes with time during the rolling process.

tion 5 is poor. In Figs. 7b–d, the fracture morphology is equiaxed dimples, and the distribution of dimples on the entire surface is relatively uniform. The material fully exhibits ductile fracture when stretched so that these positions exhibit excellent ductility.

3.4. Temperature change in the rolling process

To explain the trend of yield strength (σ_s) and tensile strength (σ_b) curves, the final rolling process and cooling process after rolling are simulated by finite element analysis. First of all, to verify the conclusion mentioned above, the temperature in the center of the steel plate is higher, while the temperature at the edge is lower. In rolling, heat transfer occurs between the plate and the roller and the environment, and the plate temperature will change. The temperature will affect the deformation resistance and material structure changes. As shown in Fig. 8, two areas are selected to correspond to the center and edge of the steel plate. The temperature variation of two areas with rolling time is derived, as shown in Fig. 9. When the plate starts rolling, the initial temperature of the plate is set

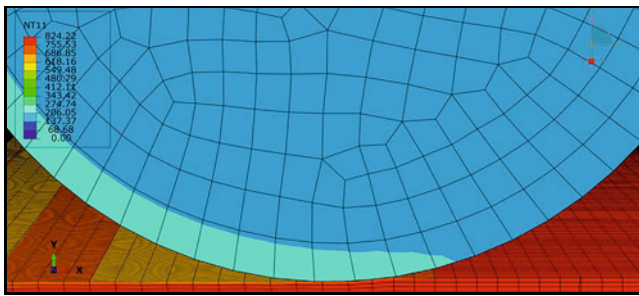


Fig. 10. The temperature change of the steel plate and roller at the beginning of contact.

at 820 °C, the initial temperature of the roll is 200 °C, and the room temperature is 20 °C. In the beginning, when the plate enters the roller, the deformation of the steel plate produces heat, and the friction between the steel plate and roller produces heat. At the same time, there will be heat transfer between the steel plate and roll. As shown in Fig. 10, when the plate contacts the roller for the first time, the plate temperature drops. The temperature decreases (the heat loss is mainly due to the heat conduction around the plate) based on convection radiation heat conduction characteristics. With the increase in the temperature gradient, the temperature decrease is more prominent. However, the effect of deformation heat generation and friction heat generation is gradually enhanced. The temperature of the contact part of the roller will increase, so there will be a temperature rising trend in the image of 0.5–1 s. After the plate leaves the roller, the temperature will decrease evenly due to the heat exchange between the plate and the air, and the trend is linear. Because the heat dissipation in the center is slower than that in the edge, the temperature will be higher. This result is consistent with the above results that the center temperature is higher than the edge temperature.

3.5. The distribution of stress and strain

In the actual production process, to reduce the defects of the edge of the plate on the quality of the finished product, it is necessary to cut the edge of the plate. Therefore, the rolling simulation results are processed as the edge of the rolled plate is cut to meet the actual production. In this paper, three transverse direction node lines on the plate surface are selected to ensure measurement accuracy, as shown in Fig. 11. The trend of the three curves is the same. We can find that the stress in the center (Position 3) is lower than that on both sides (Position 2), and the stress on the edge (Position 1) fluctuates wildly. First of all, the stress is lower for the center (Position 3), mainly due to the higher temperature in the center. The deformation resistance of the material is weaker than that of

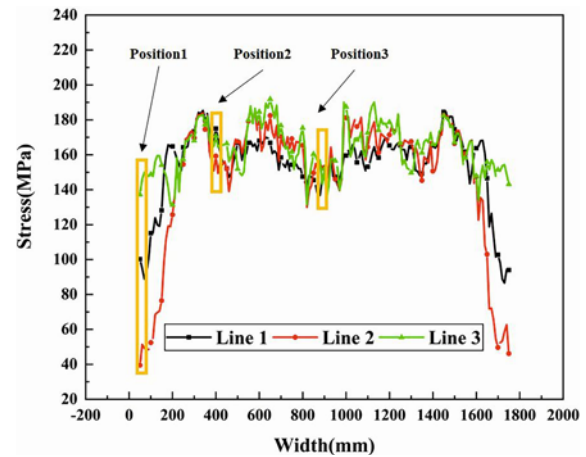


Fig. 11. The stress curves of three nodal lines along the transverse direction.

the surrounding, which makes it easier to deform in the rolling process, so the stress is lower. Therefore, Position 3 will produce greater deformation than Position 2, increasing dislocation density and strength. Next is the plate edge (Position 1). The results show that the stress at the edge is the smallest. When rolling, the edge is in the free flow area, so the deformation direction of the plate edge is the most, and the deformation in all directions cannot be accurately controlled. The edge is most prone to deformation, which may lead to wave shape and cracking and the fluctuation of mechanical properties at each edge position. Therefore, in tension, a local position of the edge (Position 1) will crack first, leading to the fracture of the whole specimen, and then the elongation of the edge sample is low. However, the grain distribution and particle size of the edge measured in the previous experiment are more uniform. According to the Hall-Petch relationship, the grain size at the edge is the smallest, and the tensile strength is higher, resulting in poor plasticity and higher strength.

As shown in Fig. 12, the strain in the center (Position 3) is relatively stable, and the value is considerable. The transverse range of the stable strain in the center is longer than that of the stress, indicating that phase occurs in the case of a stress fluctuation. With the same amount of deformation, the center is more uniform, but the internal grain distribution changes, leading to different textures and properties in different directions during uniaxial tension. The same grain orientation difference and larger grain size lead to the uneven resistance of this part to deformation, and the cracking phenomenon will occur from some weak positions. Due to the high temperature in the center, it is easier to deform, but the stress is smaller than in the surrounding two sides (Position 2), indicating that the stress is minor and the deformation is large. This indicates that the center is easy to deform and has high

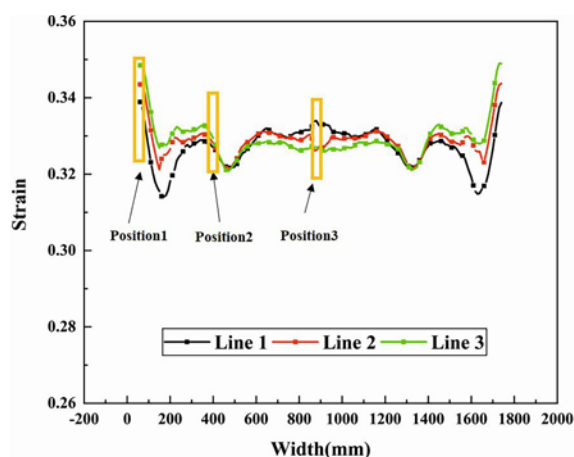


Fig. 12. The strain curves of three nodal lines along the transverse direction.

elongation. At this time, the effect of grain size on its strength is reduced, and finally, it shows a higher strength than Position 2. Then comparing the shapes of two sides (Position 2) at the center, it can be found that the strain diagram and the corresponding place in the stress diagram are in the same state of fluctuation, indicating that the flatness of the surface at both sides of the center (Position 2) is low. This leads to inhomogeneous stress in different positions due to uneven surfaces during stretching, making the material present the lowest overall tensile strength. The strain at the edge (Position 1) is the largest. Combined with the above stress, it is the case of minor stress and large strain, which indicates that it is the most accessible place to deform. Although the grain size of Position 1 is small due to the high cooling rate, the deformation of the edge is not easy to control, which makes it easier to crack in the tensile process, and there are lots of defects in the edge, which leads to the lowest elongation. However, despite the poor elongation, the strength is still the highest because of the small grain size and uniform distribution at the edge.

4. Discussion

4.1. Influence factors of transverse microstructure distribution

The effect of cooling rate on grain size is significant. With the increase in cooling rate, the ferrite grain size decreases obviously. The effect of the cooling rate after rolling on the grain size is mainly due to the cooling rate affecting the transformation process of γ (austenite) \rightarrow α (ferrite) and the growth process of ferrite grain after transformation [18]. The deformed austenite has a large undercooling degree when the cooling rate is high. The driving force of nucleation increases; the critical size of ferrite nucleation

decreases; the number of nucleation increases. Multiple nuclei grow at the same time. The grain size is acceptable. In the cooling process after phase transformation, the cooling speed is fast; the cooling time is short; ferrite grain growth is inhibited. Therefore, the ferrite grain can be refined [18, 21]. Therefore, in the production of a low-carbon steel plate, in order to refine the structure, it is necessary to cool after rolling quickly. However, the effect of the cooling rate on grain refinement is limited because the eutectoid transformation is inhibited with the increase in cooling rate.

It is also found that the grain growth of ferrite in low-carbon steel is controlled by temperature and austenite island, and there is a competitive mechanism between the two factors [22, 23]. When the annealing temperature increases, the initial grain growth rate also increases, which indicates that the grain growth is temperature-dependent. Then, when a certain amount of austenite is formed, the network structure is formed simultaneously, which hinders the migration of grain boundary and leads to a decrease in growth rate. Although the temperature increased, the growth rate decreased. This shows that the pinning effect is stronger than the temperature effect at this stage.

In the low-temperature region [22] (temperature $\leq 825^\circ\text{C}$), the effect of temperature increase on grain growth is more evident than that of the austenite island pinning effect. Therefore, the grain growth process is highly temperature-dependent in this state.

Arrhenius equation describes the relationship between diffusion coefficient and temperature:

$$D = D_0 \exp(-Q/RT), \quad (1)$$

where D_0 is the Arrhenius constant, Q is the diffusion activation energy, R is the molar gas constant, and T is the temperature [21, 23]. According to the Arrhenius equation, we can know that due to the slow heat dissipation in the center, the temperature is higher than that at the edge. Therefore, the higher the temperature is, the higher the atomic activity is, the stronger the diffusion ability of atoms is, and the easier the grain boundary is to migrate. Because the grain growth is carried out through the migration of grain boundary, the larger the grain size will be when the mobility is higher. In the same way, the cooling speed of the edge is fast, and the undercooling degree is more considerable, which increases the nucleation rate of grain and generates more grain. Because the total area remains unchanged, the final grain is smaller.

4.2. Influence factors of transverse mechanical properties

In general, the grain size and yield strength of

metallic materials can be correlated by the Hall-Petch relationship. The effect of grain size on metal strength is determined by K (Hall-Petch coefficient) value. In previous studies, reducing the grain size is the most commonly used method to improve the strength of metals and alloys. When the grain size decreases, the strength will increase, which is described by the Hall-Petch relationship [24]:

$$\sigma_s = \sigma_0 + kd^{-\frac{1}{2}}, \quad (2)$$

where σ_s is the yield strength, σ_0 is a constant, approximately equal to the yield strength of a single crystal, k is the Hall-Petch coefficient, and d is the average grain size. According to this formula, the yield strength is inversely proportional to the grain diameter. The dislocation migration at grain boundaries is the essence of Eq. (2) [24]. When dislocation migrates at the grain boundary, stress concentration occurs at the grain boundary, which will hinder the movement of dislocation. When the critical value is reached, the dislocation sources in grain boundaries or adjacent grain will be activated by stress concentration. The macro yield of polycrystalline materials is controlled by the continuous micro-plastic flow during dislocation migration in grain boundaries.

However, based on the above grain size and strength curves, we can find it slightly different from the Hall-Petch relationship. Although the grain size of Positions 2 and 4 is smaller than that of a Position 3 in the center, the strength of Positions 2 and 4 decreases, not conforming to the Hall-Petch relationship. In addition to grain size, the K value also affects the strength because it controls the initial stress concentration caused by dislocation stacking and thus controls the dislocation length acting on the dislocation source in the adjacent grain [25]. It is well known that dislocation or twin deformation mechanisms control the plastic behavior of micron grain metals. However, when the grain size is reduced to the nanoscale, graphite-based deformation mechanisms (such as graphite sliding or creep) play a significant role in the deformation [26]. When the grain size is less than 12 nm, the plastic deformation is no longer dominated by dislocation motion, but it is carried by atoms sliding in the grain boundary. When the grain boundary ratio increases, the softening effect will appear. However, it is difficult to produce a reverse Hall-Petch relationship for grain size in low-carbon steel. Therefore, the reverse Hall-Petch effect is not considered in this paper [26–28].

Because the deformation mechanism is affected by the grain size, dislocation slip is no longer the primary deformation mechanism when the grain size reaches a critical value. With the increase of grain size, the deformation mainly changes from slip to twin. Similarly, twins are controlled by grain size. The effect of grain size on twinning is usually in two ways [27, 29]. On the

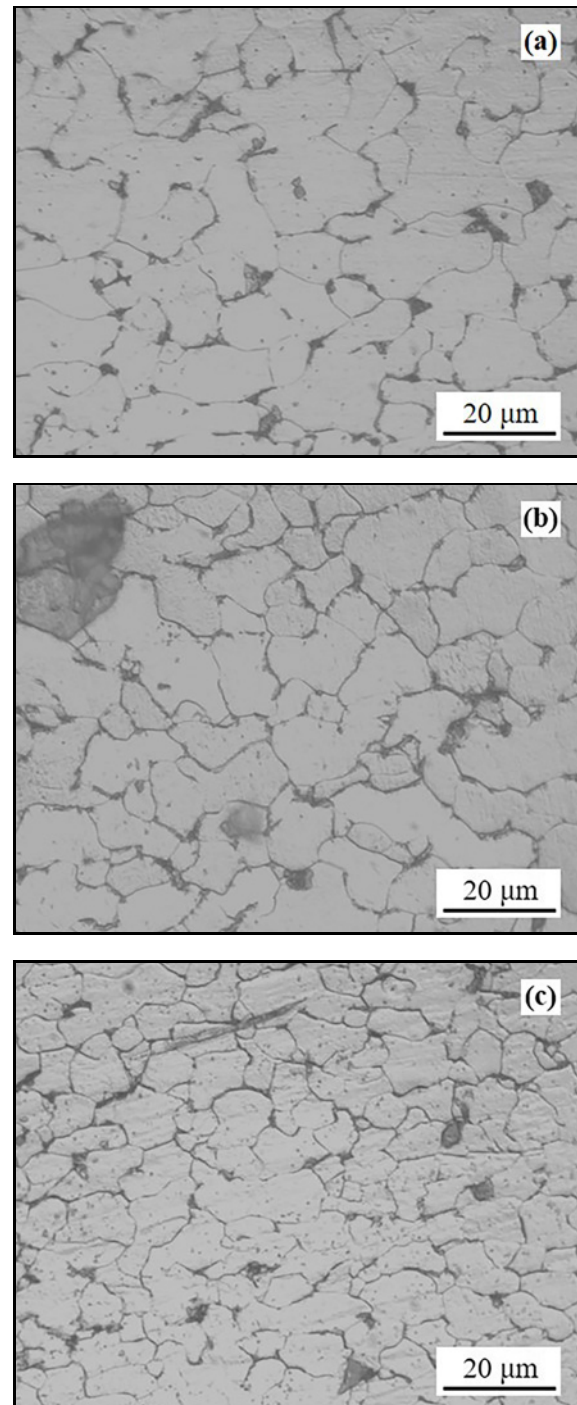


Fig. 13. High-resolution optical microstructure of hot-rolled low-carbon steel plate: (a) Position 2, (b) Position 3, and (c) Position 4.

one hand, the nucleation of twins is controlled by the stress concentration at the grain boundary. The nucleation density of twins is dominated by grain size; on the other hand, grain size affects the growth of twins. In addition, when the second phase particles, precipitates, or solutes interact with dislocation sources and

moving dislocations in the grain, the slope k in the Hall-Petch formula will increase [28]. It can be found that Position 3 has more second phases at the grain boundaries, as shown in Fig. 13. The appearance of the second phase improves the strength. It has been shown that in different metal systems containing precipitates or solute atoms, their presence leads to an increase in the K value [27]. K value is also affected by temperature. K decreases with the increase of temperature because of the decrease of CRS (critical shear stress) required to operate dislocation sources near grain boundaries and the increase of the number of active slip systems, which in turn reduces the Taylor factor and finally affects the K value [30]. The effect of plastic strain on K is realized by the generation and disappearance of dislocations in dynamic recovery [31]. The yield strength at this stage is not determined by the grain size but by the favorable crystal orientation. Due to the different position distribution of the samples in this paper, the deformation degree is different in the rolling process, and the stress and strain received are different, which eventually leads to the difference in the K value of each sample. Finally, the strength trend does not fully conform to the Hall-Petch relationship.

According to Table 1, there is more Si at the edge, which can be dissolved in ferrite and austenite to improve the hardness and strength of the steel. However, when there is more Si, the plasticity and toughness of the steel will be significantly reduced. So the ductility of the edge is poor, but the strength is the highest. Generally, when the grain size of the material is in the same order of magnitude, the yield strength and tensile strength of the material will be increased with the increase of P content [32]. This is due to replacing iron atoms with phosphorus atoms in the steel, which stores a large amount of distortion energy in the material, increasing strength. As shown in Table 1 and Fig. 6b, the P content of Position 2 is more similar to the grain size of Position 4, so the strength of Position 2 is higher than that of other positions. According to Fig. 6e, it can be found that the fracture morphology of Position 5 is layered, and the morphology on the left and right is inconsistent. As is known, the segregation of P leads to delamination that eventually increases the brittleness of the steel. P content of Position 5 is the highest, so Position 5 shows the worst ductility. P is enriched at grain boundaries. The more grain boundaries, the greater the enrichment is. Due to the smallest grain size at the edge, a large amount of P is enriched at the edge. Because phosphorus can weaken the grain boundary when the enrichment of phosphorus is higher, the material's brittleness will increase, and the brittle fracture trend will be increased eventually. There are two main reasons for grain boundary embrittlement caused by phosphorus segregation. The first reason is to change the bond

between local atoms, thus changing the fracture energy. The second reason is to change the dislocation in the local area, that is, to change the interaction between the grain boundaries. The researchers [33] studied the relationship between grain size and ductility based on simulation and experiment. The results show that there is a threshold of grain size. When the grain size is smaller than the threshold, the ductility increases with the grain size. For the same fracture mode, the effect of grain size on fracture strain is limited. As shown in Figs. 6c,e, the ductility is improved when the fracture mode changes from brittle fracture to uniform plastic fracture. Other researchers [34] have shown that steels with larger grain sizes than other steels have better ductility. So Position 3 shows better ductility than Position 1 and Position 5. Therefore, the element content and grain size in the material jointly control the strength and toughness.

5. Summary and conclusions

The microstructure observation, mechanical property analysis, and finite element simulation were used to observe transverse grain size and fracture surface morphology of hot-rolled low-carbon steel plate. The hardness, strength, cooling rate, stress, and strain were also studied. The following conclusions have been made:

(1) The transverse structure and properties of the hot-rolled steel sheet are inhomogeneous. The center grain size is large, the hardness is low, the edge grain size is small, and the hardness is high.

(2) The center position contains less phosphorus and silicon, and the fracture morphology shows uniform equiaxed dimples and a large number of second phases, so it has good ductility and high strength.

(3) Finite element simulation showed that the inhomogeneity between the middle and the edge is related to the different cooling rates.

(4) The tensile and yield strength curves along the transverse direction are similar to the W shape. The highest strength is at the edge, the second at the center, and the lowest at both sides of the center. The center plasticity of the alloy is the highest, and the edge plasticity is the worst, mainly due to the synergy between the alloying elements and the grain size.

Acknowledgements

The work is supported by the Innovation Research Group of universities in Chongqing (CXQT21030), Chongqing Talents: Exceptional Young Talents Project (CQYC 201905 100).

References

- [1] A. M. Beltrán-Zúñiga, L. J. González-Velázquez, I. D. Rivas-López, F. Hernández-Santiago, J. H. Dorantes-Rosales, V. M. López-Hirata, Determination of fracture toughness in the short transverse direction of low carbon steel pipes by compact-tension specimens completed by welded attachments, *Eng. Fract. Mech.* 222 (2019) 106711. <https://doi.org/10.1016/j.engfracmech.2019.106711>
- [2] L. Zhao, L. Qian, Q. Zhou, D. Li, J. Meng, The combining effects of ausforming and below-*M_s* or above-*M_s* austempering on the transformation kinetics, microstructure and mechanical properties of low-carbon bainitic steel, *Mater. Des.* 183 (2019) 108123. <https://doi.org/10.1016/j.matdes.2019.108123>
- [3] L. Zhao, N. Park, Y. Tian, S. Chen, A. Shibata, N. Tsuji, Novel thermomechanical processing methods for achieving ultragrain refinement of low-carbon steel without heavy plastic deformation, *Mater. Res. Lett.* 5 (2017) 61–68. <https://doi.org/10.1080/21663831.2016.1208301>
- [4] Y. Li, W. Li, M. Na, W. Liu, X. Jin, Effects of hot/cold deformation on the microstructures and mechanical properties of ultra-low carbon medium manganese quenching-partitioning-tempering steels, *Acta Mater.* 139 (2017) 96–108. <https://doi.org/10.1016/j.actamat.2017.08.003>
- [5] M. Wu, W. Fang, R.-M. Chen, B. Jiang, H.-B. Wang, Y.-Z. Liu, H.-L. Liang, Mechanical anisotropy and local ductility in transverse tensile deformation in hot-rolled steels: The role of MnS inclusions, *Mater. Sci. Eng. A* 744 (2019) 324–334. <https://doi.org/10.1016/j.msea.2018.12.026>
- [6] K. M. Min, W. Jeong, S. H. Hong, C. A. Lee, P.-R. Cha, H. N. Han, M.-G. Lee, Integrated crystal plasticity and phase field model for prediction of recrystallization texture and anisotropic mechanical properties of cold-rolled ultra-low carbon steels, *Int. J. Plast.* 127 (2019) 102644. <https://doi.org/10.1016/j.iiplas.2019.102644>
- [7] L. Cheng, K. M. Wu, New insights into intragranular ferrite in a low-carbon low-alloy steel, *Acta Mater.* 57 (2009) 3754–3762. <https://doi.org/10.1016/j.actamat.2009.04.045>
- [8] F. Haddadi, J.-W. Cho, S. Y. Lee, The effect of chemical composition on grain structure and texture evolution of hot rough rolled carbon steels, *Mater. Sci. Eng. A* 607 (2014) 102–112. <https://doi.org/10.1016/j.msea.2014.03.072>
- [9] J. Chen, M. Lv, S. Tang, Z. Liu, G. Wang, Correlation between mechanical properties and retained austenite characteristics in a low-carbon medium manganese alloyed steel plate, *Mater. Character.* 106 (2015) 108–111. <https://doi.org/10.1016/j.matchar.2015.05.026>
- [10] T. Hayashi, S. Morito, T. Ohba, Local distribution of orientation relationship and microstructure evolution of lath martensite in an ultra-low-carbon steel, *Scr. Mater.* 180 (2020) 1–5. <https://doi.org/10.1016/j.scriptamat.2020.01.011>
- [11] Y. Zhang, H. Zhang, G. Wang, S. Hu, Application of mathematical model for microstructure and mechanical property of hot rolled wire rods, *Appl. Math. Model.* 33 (2009) 1259–1269. <https://doi.org/10.1016/j.apm.2008.01.024>
- [12] A. Mukhopadhyay, A. Iqbal, Prediction of mechanical properties of hot rolled, low-carbon steel strips using artificial neural network, *Mater. Manuf. Processes* 20 (2005) 793–812. <https://doi.org/10.1081/AMP-200055140>
- [13] R. B. Mei, L. I. Chang-Sheng, X. H. Liu, B. Han, Analysis of strip temperature in hot rolling process by finite element method, *J. Iron Steel Res. Int.* 17 (2010) 17–21. [https://doi.org/10.1016/S1006-706X\(10\)60052-0](https://doi.org/10.1016/S1006-706X(10)60052-0)
- [14] C. Yang, P. Liu, Y. Luan, D. Li, Y. Li, Study on transverse-longitudinal fatigue properties and their effective-inclusion-size mechanism of hot rolled bearing steel with rare earth addition, *Int. J. Fatigue* 128 (2019) 105193. <https://doi.org/10.1016/j.ijfatigue.2019.105193>
- [15] X. Yun, L. Gardner, Stress-strain curves for hot-rolled steels, *J. Constr. Steel. Res.* 133 (2017) 36–46. <https://doi.org/10.1016/j.jcsr.2017.01.024>
- [16] K.-M. Lee, H.-C. Lee, Grain refinement and mechanical properties of asymmetrically rolled low carbon steel, *J. Mater. Process. Technol.* 210 (2010) 1574–1579. <https://doi.org/10.1016/j.jmatprotec.2010.05.004>
- [17] F. A. Mirza, A. Macwan, S. D. Bhole, D. L. Chen, X.-G. Chen, Microstructure, tensile and fatigue properties of ultrasonic spot welded aluminum to galvanized high-strength-low-alloy and low-carbon steel sheets, *Mater. Sci. Eng. A* 690 (2017) 323–336. <https://doi.org/10.1016/j.msea.2017.03.023>
- [18] M. Umamoto, Zing Hai Guo, I. Tamura, Effect of cooling rate on grain size of ferrite in a carbon steel, *Mater. Sci. Technol.* 3 (1987) 249–255. <https://doi.org/10.1179/mst.1987.3.4.249>
- [19] F. H. Samuel, S. Yue, J. J. Jonas, K. R. Barnes, Effect of dynamic recrystallization on microstructural evolution during strip rolling, *ISIJ Int.* 30 (1990) 216–225. <https://doi.org/10.2355/isijinternational.30.216>
- [20] X.-X. Lu, F. Li, X.-D. Cao, S.-M. Zhao, Research on the stress-strain curve of plain carbon steel Q235, *Shandong Metall.* 1 (2007) 41–42. <https://doi.org/10.16727/j.cnki.issn1004-4620.2007.01.021>
- [21] M. Esmailian, The effect of cooling rate and austenite grain size on the austenite to ferrite transformation temperature and different ferrite morphologies in microalloyed steels, *Iran. J. Mater. Sci. Eng.* 7 (2010) 7–14.
- [22] F. Najafkhani, H. Mirzadeh, M. Zamani, Effect of intercritical annealing conditions on grain growth kinetics of dual phase steel, *Met. Mater. Int.* 25 (2019) 1039–1046. <https://doi.org/10.1007/s12540-019-00241-2>
- [23] Y. J. Lan, D. Z. Li, Y. Y. Li, Modeling austenite decomposition into ferrite at different cooling rate in low-carbon steel with cellular automaton method, *Acta Mater.* 52 (2004) 1721–1729. <https://doi.org/10.1016/j.actamat.2003.12.045>
- [24] E. O. Hall, The deformation and ageing of mild steel: II. Characteristics of the Lüders deformation, *Proc. Phys. Soc. B* 64 (1951) 742. <https://doi.org/10.1088/0370-1301/64/9/302>
- [25] Z. C. Cordero, B. E. Knight, Ch. A. Schuh, Six decades of the Hall-Petch effect – a survey of grain-size strengthening studies on pure metals, *Int. Mater. Rev.* 61 (2016) 495–512. <https://doi.org/10.1080/09506608.2016.1191808>

- [26] D. Tian, C.-J. Zhou, J.-H. He, Hall-Petch effect and inverse Hall-Petch effect: A fractal unification, *Fractals* 26 (2018) 1850083. <https://doi.org/10.1142/S0218348X18500834>
- [27] D. Zhou, H. Wang, D. W. Saxey, O. Muránsky, D. Zhang, Hall-Petch slope in ultrafine grained Al-Mg alloys, *Metall. Mater. Trans. A* 50 (2019) 4047–4057. <https://doi.org/10.1007/s11661-019-05329-3>
- [28] H. Yu, Y. Xin, M. Wang, Q. Liu, Hall-Petch relationship in Mg alloys: A review, *J. Mater. Sci. Technol.* 34 (2018) 248–256. <https://doi.org/10.1016/j.jmst.2017.07.022>
- [29] N. Hansen, Hall-Petch relation and boundary strengthening, *Scr. Mater.* 51 (2004) 80–806. <https://doi.org/10.1016/j.scriptamat.2004.06.002>
- [30] S. Chen, K. K. Tseng, Y. Tong, W. Li, P. K. Liaw, Grain growth and Hall-Petch relationship in a refractory HfNbTaZrTi high-entropy alloy, *J. Alloys Compd.* 795 (2019) 19–26. <https://doi.org/10.1016/j.jallcom.2019.04.291>
- [31] S. V. Astafurov, G. G. Maier, E. V. Melnikov, V. A. Moskvina, M. Y. Panchenko, E. G. Astafurova, The strain-rate dependence of the Hall-Petch effect in two austenitic stainless steels with different stacking fault energies, *Mater. Sci. Eng. A* 756 (2019) 365–372. <https://doi.org/10.1016/j.msea.2019.06.010>
- [32] S. J. Jia, Q. U. Peng, Y. Weng, J. B. Zhang, H. J. Chen, Q. Y. Liu, Research on influence of phosphorus and grain size on mechanical properties of low carbon steels, *Iron Steel* 40 (2005) 59–63.
- [33] X. Shang, H. Zhang, Z. Cui, M. W. Fu, J. Shao, A multiscale investigation into the effect of grain size on void evolution and ductile fracture: Experiments and crystal plasticity modeling, *Int. J. Plast.* 125 (2020) 133–149. <https://doi.org/10.1016/j.ijplas.2019.09.009>
- [34] J. K. Hwang, Effect of grain size on tensile and wire drawing behaviors in twinning-induced plasticity steel, *Mater. Sci. Eng. A* 772 (2020) 138709. <https://doi.org/10.1016/j.msea.2019.138709>